

Article

New Mixed $Y_{0.5}R_{0.5}VO_4$ and $RVO_4:Bi$ Materials: Synthesis, Crystal Structure and Some Luminescence Properties

Leonid Vasylechko ^{1,*}, Andrii Tupys ^{1,2}, Vasyl Hreb ¹ , Volodymyr Tsiumra ^{3,4}, Iryna Lutsiuk ¹ and Yaroslav Zhydachevskyy ^{1,4}

¹ Semiconductor Electronics Department, Lviv Polytechnic National University, 12 Bandera Str., 79013 Lviv, Ukraine; andriytupys@ukr.net (A.T.); wasiahreb@meta.ua (V.H.); ira_lutsuk@ukr.net (I.L.); zhydach@ifpan.edu.pl (Y.Z.)

² Natural Sciences College, Ivan Franko National University of Lviv, 79016 Lviv, Ukraine

³ Department of Experimental Physics, Ivan Franko National University of Lviv, 79016 Lviv, Ukraine; tsiumra@ifpan.edu.pl

⁴ Institute of Physics, Polish Academy of Sciences, Al. Lotników 32/46, 02 668 Warsaw, Poland

* Correspondence: crystal-lov@polynet.lviv.ua; Tel: +38-032-2582696

Received: 25 July 2018; Accepted: 7 September 2018; Published: 10 September 2018



Abstract: The results are reported on a precise crystal structure and microstructure determination of new mixed YVO_4 -based orthovanadates of $Y_{0.5}R_{0.5}VO_4$ ($R = Sm, Tb, Dy, Ho, Tm, Yb, Lu$) as well as some Bi^{3+} -doped RVO_4 ($R = La, Gd, Y, Lu$) nano- (submicro-) materials. The formation of continuous solid solutions in the YVO_4 – RVO_4 pseudo-binary systems ($R = Sm, Tb, Dy, Ho, Tm, Yb, Lu$) has been proved. The lattice constants and unit cell volumes of the new mixed orthovanadates were analyzed as a function of R^{3+} cation radius. The impact of crystal structure parameters on the energy band gap of the materials was studied by means of photoluminescence studies of the Bi^{3+} -doped compounds.

Keywords: mixed orthovanadates; RVO_4 ; Bi^{3+} ; crystal structure; microstructure; photoluminescence

1. Introduction

Rare earth (RE) orthovanadates RVO_4 with monazite and zircon type structures have been widely studied in the last decades due to their important properties. They are used as laser host materials and optical polarizers, gas sensors, thin film phosphors and catalysts (see [1–3] and references therein). Recently, mixed RE orthovanadates were proposed as new class of stimulated Raman scattering (SRS)-active crystals [4]. Nowadays, the rare earth orthovanadates doped with Bi^{3+} ions are of great importance in modern electronics because of their unique luminescent properties. Moreover, co-doping with other RE causes the change in color of luminescence, e.g., from red to green [5]. Recently, yttrium–scandium–niobium vanadates doped with Bi^{3+} ions were proposed as phosphors perspective for white LEDs due to the possibility of tuning of their photoluminescence color over the whole visible range [6]. Besides, these kinds of solid solutions were proved to be effective photocatalysts for overall water splitting under UV light [7] and UV-absorbing luminescent converters to enhance the power conversion efficiency and photochemical stability of solar cells [8]. Just recently an extensive review article, which includes a comprehensive survey of the diverse application fields of RVO_4 -based materials, was published in Reference [9].

Among all RVO_4 orthovanadates, the YVO_4 -based materials are undoubtedly the most studied, substantially due to its two principal applications as active laser medium used in diode-pumped solid-state lasers and the dominant red phosphor used in cathode ray tubes. However, in spite of increasing number of publications on the mixed orthovanadates in the last decades, detailed structural

information for the mixed $Y_{1-x}R_xVO_4$ materials is rather limited. To the best of our knowledge, full structural data are available only for the compositions with “light” rare earths (La, Ce, Pr, Nd, Sm, Eu and Gd) [10,11]. Among corresponding representatives of the “heavy” RE, structural data are reported only for $Y_{0.25}Er_{0.75}VO_4$ [12].

Therefore, the main aim of the present study is the synthesis and precise crystal structural characterization of new mixed YVO_4 -based orthovanadates $Y_{0.5}R_{0.5}VO_4$ ($R = Sm, Tb, Dy, Ho, Tm, Yb, Lu$), as well as some Bi^{3+} -doped RVO_4 materials ($R = Gd, Y, Y_{0.5}Lu_{0.5}, Lu$), which were studied in order to reveal an impact of structural parameters on energy band gap and photoluminescence properties.

2. Results and Discussion

2.1. Crystal Structure Results

2.1.1. Mixed Vanadates $Y_{0.5}R_{0.5}VO_4$

According to X-ray powder diffraction examination, all the $Y_{0.5}R_{0.5}VO_4$ ($R = Sm, Tb, Dy, Ho, Tm, Yb, Lu$) vanadates adopt tetragonal zircon-type structures (Figure 1). No traces of the impurity phases were detected. Detectable broadening of the diffraction maxima is evidently associated with the microstrains $\langle \varepsilon \rangle$ caused by dispersion of interplanar distances $\langle \Delta d \rangle / d$ and possible nano-crystalline nature of the powders obtained. The colour of the $Y_{0.5}R_{0.5}VO_4$ samples synthesized at 1273 K varied between tan or beige, depending on composition.

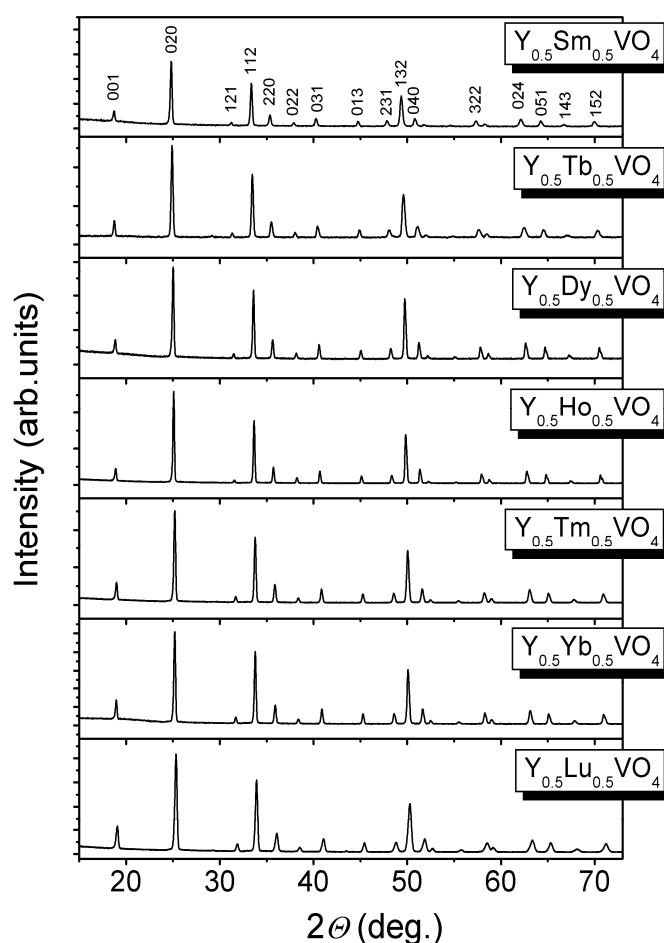


Figure 1. Representative parts of XRD patterns of the $Y_{0.5}R_{0.5}VO_4$ ($R = Sm, Tb, Dy, Ho, Tm, Yb, Lu$) samples. The Miller indices are given for the zircon-type structure.

Phase purity and crystal structure of the materials synthesized were further proved by the full profile Rietveld refinement technique. As a starting model for the refinement, the atomic positions in the YVO_4 structure obtained from neutron powder diffraction data were used [13]. The Y and R atoms are assuming to occupy the same $4a$ atomic positions in $Y_{0.5}R_{0.5}VO_4$ structures in a random way. In the refinement procedure, the lattice constants, positions of oxygens and displacement parameters of all atoms (adp's) were refined together with profile parameters and corrections for the adsorption and instrumental sample shift. In all cases, an excellent fit between calculated and experimental diffraction profiles was obtained. As an example, Figure 2 demonstrates graphical results of Rietveld refinement of $Y_{0.5}Sm_{0.5}VO_4$ structure in space group $I4_1/amd$.

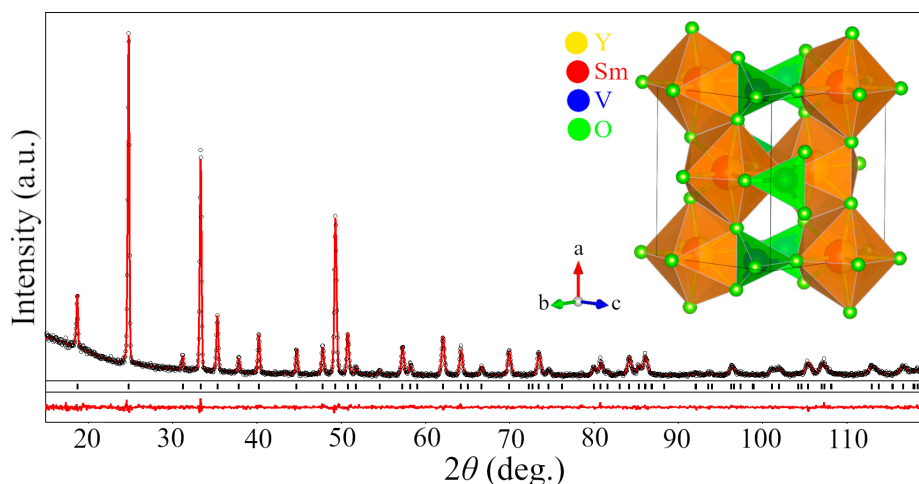


Figure 2. Graphical results of Rietveld refinement of $Y_{0.5}Sm_{0.5}VO_4$ structure. Experimental XRD pattern (black circles) is shown in comparison with the calculated profile (red line). Short vertical bars indicate positions of Bragg's maxima in space group $I4_1/amd$. Inset shows visualization of $Y_{0.5}Sm_{0.5}VO_4$ zircon-type structure as chains of alternating VO_4 tetrahedra and Y/SmO_8 polyhedra.

The refined structural parameters of the $Y_{0.5}R_{0.5}VO_4$ ($R = Sm, Tb, Dy, Ho, Tm, Yb, Lu$) solid solutions and corresponding interatomic distances and angles in the zircon-type $Y_{0.5}R_{0.5}VO_4$ structures are summarized in Tables 1 and 2, respectively.

Table 1. Lattice parameters, fractional coordinates and isotropic adp's in $Y_{0.5}R_{0.5}VO_4$ series and microstructural parameters of corresponding powders. Space group $I4_1/amd$; Y(R) in $4a$ ($0\ 3/4\ 1/8$); V in $4b$ ($0\ 1/4\ 3/8$), O in $16h$ ($0\ y\ z$).

| Parameters, Residuals | R in $Y_{0.5}R_{0.5}VO_4$ | | | | | | |
|-----------------------------------|---------------------------|-----------|-----------|-----------|-----------|-----------|-----------|
| | Sm | Tb | Dy | Ho | Tm | Yb | Lu |
| $a, \text{Å}$ | 7.1933(4) | 7.1509(3) | 7.1337(2) | 7.1206(1) | 7.0907(2) | 7.0815(1) | 7.0655(2) |
| $c, \text{Å}$ | 6.3398(4) | 6.3126(3) | 6.2991(2) | 6.2901(1) | 6.2724(2) | 6.2684(2) | 6.2588(2) |
| $V, \text{Å}^3$ | 328.05(5) | 322.79(5) | 320.56(2) | 318.92(2) | 315.36(2) | 314.35(2) | 312.45(3) |
| $B_{iso}(Y/R), \text{Å}^2$ | 0.59(4) | 0.62(3) | 0.78(3) | 1.17(3) | 0.88(2) | 0.84(2) | 0.67(2) |
| $B_{iso}(V), \text{Å}^2$ | 0.71(12) | 0.45(7) | 0.64(6) | 0.48(5) | 0.80(4) | 0.65(4) | 0.52(4) |
| $y/b(O)$ | 0.4302(13) | 0.4278(7) | 0.4313(6) | 0.4308(5) | 0.4312(4) | 0.4320(5) | 0.4321(4) |
| $z/c(O)$ | 0.2033(13) | 0.2071(7) | 0.2048(7) | 0.2054(5) | 0.2040(4) | 0.2062(5) | 0.2034(4) |
| $B_{iso}(O), \text{Å}^2$ | 1.1(3) | 1.42(15) | 1.55(14) | 1.29(10) | 1.48(8) | 1.38(9) | 1.51(9) |
| R_I | 0.030 | 0.029 | 0.021 | 0.023 | 0.022 | 0.029 | 0.023 |
| R_P | 0.124 | 0.129 | 0.095 | 0.080 | 0.082 | 0.073 | 0.085 |
| D, nm | 108 | 202 | 92 | 158 | 106 | 129 | 93 |
| $\langle \varepsilon \rangle, \%$ | 0.121 | 0.185 | 0.032 | 0.039 | 0.090 | 0.065 | 0.207 |
| R | 0.014 | 0.045 | 0.003 | 0.042 | 0.003 | 0.006 | 0.044 |

Table 2. Selected interatomic distances (Å) and angles (°) in $Y_{0.5}R_{0.5}VO_4$ structures.

| | Sm | Tb | Dy | Ho | Tm | Yb | Lu |
|----------------------------|-----------|-----------|-----------|-----------|-----------|-----------|-----------|
| VO ₄ tetrahedra | | | | | | | |
| V–O × 4 | 1.693(9) | 1.656(10) | 1.680(7) | 1.673(8) | 1.673(6) | 1.665(8) | 1.675(8) |
| O··O × 4 | 2.846(11) | 2.781(6) | 2.816(9) | 2.811(10) | 2.811(8) | 2.789(10) | 2.813(10) |
| O··O × 2 | 2.593(13) | 2.543(7) | 2.590(10) | 2.567(12) | 2.568(9) | 2.571(12) | 2.571(12) |
| O–V–O × 4 | 114.41(3) | 114.22(2) | 113.93(3) | 114.30(3) | 114.27(3) | 113.81(3) | 114.26(3) |
| O–V–O × 2 | 99.99(3) | 100.34(2) | 100.88(3) | 100.20(3) | 100.25(3) | 101.11(3) | 100.27(3) |
| RO ₈ polyhedra | | | | | | | |
| R–O × 4 | 2.353(9) | 2.361(11) | 2.328(7) | 2.331(8) | 2.315(7) | 2.312(8) | 2.300(8) |
| R–O × 4 | 2.453(9) | 2.452(10) | 2.450(7) | 2.437(8) | 2.430(6) | 2.442(8) | 2.425(8) |
| O··O × 2 | 2.593(13) | 2.543(7) | 2.590(10) | 2.567(12) | 2.568(9) | 2.571(12) | 2.571(12) |
| O··O × 4 | 2.767(11) | 2.810 (6) | 2.763(10) | 2.757(11) | 2.739(9) | 2.762(11) | 2.723(11) |
| O··O × 8 | 3.080(10) | 3.069(5) | 3.053(8) | 3.050(9) | 3.037(7) | 3.032(9) | 3.025(9) |
| O··O × 4 | 3.401(9) | 3.419(5) | 3.368(8) | 3.371(8) | 3.348(7) | 3.348(9) | 3.326(9) |
| O–R–O × 2 | 63.83(2) | 62.49(13) | 63.81(2) | 63.55(2) | 63.80(2) | 63.52(2) | 64.03(2) |
| O–R–O × 4 | 70.27(2) | 71.42(13) | 70.63(2) | 70.60(2) | 70.46(2) | 70.97(2) | 70.31(2) |
| O–R–O × 8 | 79.68(2) | 79.20(13) | 79.38(2) | 79.50(2) | 79.53(2) | 79.20(2) | 79.57(2) |
| O–R–O × 4 | 92.55(3) | 92.75(13) | 92.70(2) | 92.63(2) | 92.62(2) | 92.78(2) | 92.61(2) |

Table 1 contains also the values of average grain size, D , and microstrains $\langle \varepsilon \rangle = \langle \Delta d \rangle / d$, evaluated from the analysis of angular dependence of XRD peak broadening by using full profile refinement procedure. The smallest grain size (92–93 nm) was detected in the $Y_{0.5}Dy_{0.5}VO_4$ and $Y_{0.5}Lu_{0.5}VO_4$ materials, whereas the biggest one (202 nm)—in $Y_{0.5}Tb_{0.5}VO_4$ sample. No obvious dependence of the grain size on the sample composition was observed. The obtained microstrain values $\langle \Delta d \rangle / d$ are varied over the range of 0.032–0.207%, predictable being lower for the $Y_{0.5}Dy_{0.5}VO_4$ and $Y_{0.5}Ho_{0.5}VO_4$ materials due to minor mismatch in ionic radii between Y^{3+} ions and Dy^{3+} or Ho^{3+} species.

The obtained structural parameters of the $Y_{0.5}R_{0.5}VO_4$ ($R = Sm, Tb, Dy, Ho, Tm, Yb, Lu$) solid solutions agree well with the literature data for the parent YVO_4 and RVO_4 compounds [13,14]. Figure 3 demonstrates evolution of the unit cell dimensions of the $Y_{0.5}R_{0.5}VO_4$ materials synthesized in comparison with the known data for pure RVO_4 compounds proving the formation of continuous solid solutions in the YVO_4 – RVO_4 pseudo-binary systems.

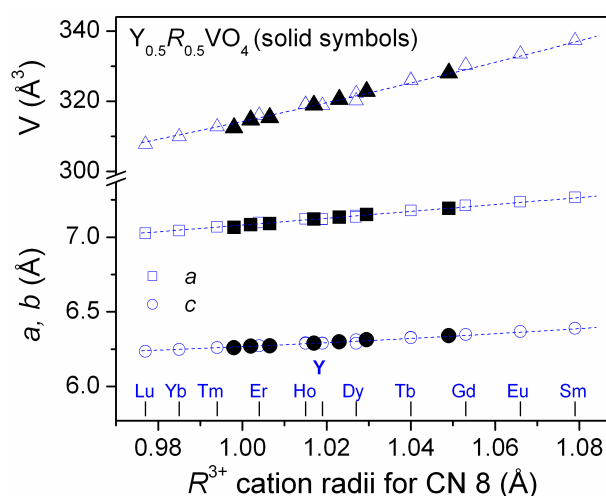


Figure 3. Lattice parameters and unit cell volumes of the $Y_{0.5}R_{0.5}VO_4$ ($R = Sm, Tb, Dy, Ho, Tm, Yb, Lu$) series (solid symbols) and the parent RVO_4 compounds [13,14] (open symbols) as a function of eight-coordinated R^{3+} cations after Shannon [15].

2.1.2. Bi³⁺-Doped Vanadates RVO₄ (R = La, Gd, Y, Y_{0.5}Lu_{0.5}, Lu)

The analysis of XRD patterns of the synthesized Bi-doped vanadates revealed a monazite-type monoclinic structure of LaVO₄:Bi and zircon-type tetragonal structure of all other RVO₄:Bi (R = Gd, Y, Y_{0.5}Lu_{0.5}, Lu) materials (Figure 4). No detectable amount of the foreign phase(s) was detected within the sensitivity limits of the technique used.

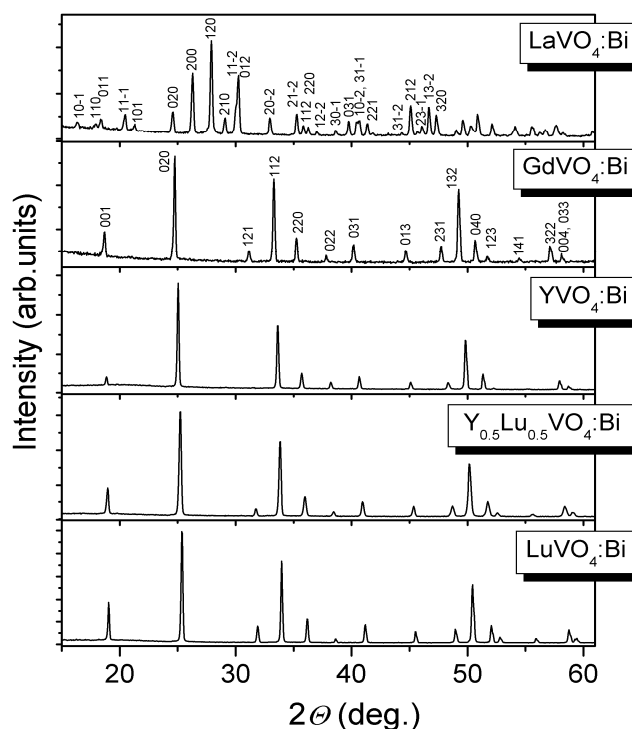


Figure 4. Representative parts of XRD patterns of the Bi³⁺-doped orthovanadates RVO₄. The Miller indices are given for the monazite-type LaVO₄:Bi and zircon-type RVO₄:Bi structures.

The full profile Rietveld refinement confirms phase purity and crystal structure of the synthesized RVO₄:Bi materials (Figure 5). Atomic positions in the monoclinic LaVO₄ [16] and tetragonal YVO₄ [13] structures were used as starting models for the refinement of corresponding Bi³⁺-doped orthovanadates. In the refinement procedure it was assumed that Bi³⁺ species partially substitute R³⁺ cations in the corresponding structures. Refinement of the lattice parameters, positional and displacement parameters of atoms together with profile parameters in space groups *P2₁/n* for LaVO₄:Bi and *I4₁/amd* for other RVO₄:Bi materials shows excellent agreement between calculated and experimental diffraction profiles (see Figure 5 as an example) and led to final structural parameters and residuals presented in Table 3.

Evaluation of microstructural parameters of Bi-doped materials lead to the average grain size, *D*, of 145, 138, 207 and 251 nm for the LaVO₄:Bi, GdVO₄:Bi, YVO₄:Bi and LuVO₄:Bi samples (Table 3). The smaller *D* values of 98 nm is observed for the mixed yttrium-lutetium vanadate (Y,Lu)VO₄:Bi. In comparison with “single rare earth” vanadates RVO₄:Bi, the latest material also shows considerably higher values of microstrains $\langle \epsilon \rangle$ (Table 3) due to significant dispersion of interplanar distances $\langle \Delta d \rangle / d$.

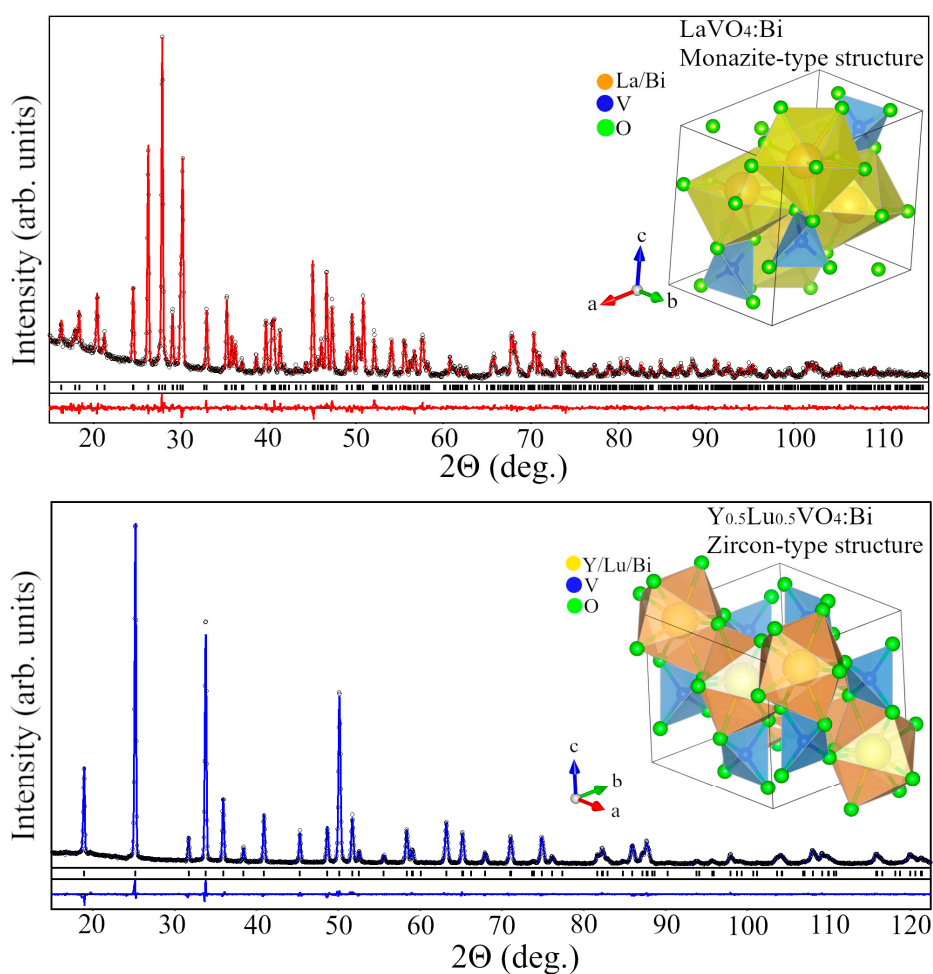


Figure 5. Graphical results of Rietveld refinement of Bi-doped LaVO_4 (**top**) and $\text{Y}_{0.5}\text{Lu}_{0.5}\text{VO}_4$ (**bottom**) structures. Experimental XRD patterns (black circles) are shown in comparison with the calculated profiles (red and blue lines, respectively). Short vertical bars on the top and bottom panels indicate positions of Bragg's maxima in the monoclinic $P2_1/n$ and tetragonal $I4_1/amd$ structures, respectively. Insets show polyhedral views of monazite-type $\text{LaVO}_4\text{:Bi}$ and zircon-type $\text{Y}_{0.5}\text{Lu}_{0.5}\text{VO}_4\text{:Bi}$ structures.

2.2. Luminescence and Optical Studies of the Bi-Doped Materials

The colour of the $\text{RVO}_4\text{:Bi}$ materials obtained depends on the sample composition and annealing temperature and varies between white or slightly yellowish to tan. The Y- and Lu-based $\text{RVO}_4\text{:Bi}$ vanadates prepared at 1073 K were white or slightly yellowish, whereas $\text{LaVO}_4\text{:Bi}$ and $\text{GdVO}_4\text{:Bi}$ materials synthesized at 1273 K were brownish evidently due to the partial formation of mixed-valence compounds [17]. It was reported [18] that there is a linear dependence between the intensity of yellow coloration of YVO_4 and the EPR signal of V^{4+} ion adjacent to an oxygen vacancy. The increase of V^{4+} ion content quenches the luminescence of the prepared samples. Therefore before the luminescence measuring the samples were washed with 0.1 M water solution of NaOH as it is recommended in the literature [19] to eliminate these adverse phenomena.

Table 3. Lattice parameters, fractional coordinates and isotropic displacement parameters in $RVO_4:Bi$ structures and corresponding microstructural parameters of the powders.

| Lattice Parameters, Residuals | Atoms, Sites | x/a | y/b | z/c | $B_{iso/eq}$, Å ² |
|---|--------------|-----------|------------|------------|-------------------------------|
| LaVO ₄ :Bi, space group $P2_1/n$ ($D = 145$ nm; $\langle \epsilon \rangle = 0.048\%$) | | | | | |
| | La/Bi, 4e | 0.2768(3) | 0.1574(4) | 0.1037(4) | 0.97(3) |
| $a = 7.0396(2)$ Å | V, 4e | 0.3013(9) | 0.1643(11) | 0.6170(10) | 0.82(11) |
| $b = 7.2777(3)$ Å | O1, 4e | 0.253(3) | 0.008(3) | 0.431(3) | 0.5(5) |
| $c = 6.7212(2)$ Å | O2, 4e | 0.384(3) | 0.344(4) | 0.496(3) | 1.1(4) |
| $\beta = 104.856(2)^\circ$ | O3, 4e | 0.478(3) | 0.099(3) | 0.826(3) | 1.4(5) |
| | O4, 4e | 0.118(3) | 0.218(3) | 0.729(3) | 2.2(6) |
| $R_I = 0.031$; $R_p = 0.122$ | | | | | |
| GdVO ₄ :Bi, space group $I4_1/amd$ ($D = 138$ nm; $\langle \epsilon \rangle = 0.020\%$) | | | | | |
| | Gd/Bi, 4a | 0 | 3/4 | 1/8 | 0.95(9) |
| $a = 7.2118(4)$ Å | V, 4b | 0 | 1/4 | 3/8 | 1.0(3) |
| $c = 6.3484(4)$ Å | O1, 16h | 0 | 0.433(2) | 0.206(2) | 0.5(4) |
| $R_I = 0.029$; $R_p = 0.167$ | | | | | |
| YVO ₄ :Bi, space group $I4_1/amd$ ($D = 207$ nm; $\langle \epsilon \rangle = 0.032\%$) | | | | | |
| | Y/Bi, 4a | 0 | 3/4 | 1/8 | 1.20(4) |
| $a = 7.1188(1)$ Å | V, 4b | 0 | 1/4 | 3/8 | 0.47(7) |
| $c = 6.2902(2)$ Å | O1, 16h | 0 | 0.4319(7) | 0.2096(7) | 1.60(13) |
| $R_I = 0.035$; $R_p = 0.076$ | | | | | |
| LuVO ₄ :Bi, space group $I4_1/amd$ ($D = 251$ nm; $\langle \epsilon \rangle = 0.037\%$) | | | | | |
| | Lu/Bi, 4a | 0 | 3/4 | 1/8 | 1.47(2) |
| $a = 7.0269(1)$ Å | V, 4b | 0 | 1/4 | 3/8 | 0.40(6) |
| $c = 6.2341(1)$ Å | O1, 16h | 0 | 0.4252(8) | 0.2117(9) | 1.63(15) |
| $R_I = 0.035$; $R_p = 0.069$ | | | | | |
| (Y,Lu)VO ₄ :Bi, space group $I4_1/amd$ ($D = 98$ nm; $\langle \epsilon \rangle = 0.095\%$) | | | | | |
| | Y/Lu/Bi, 4a | 0 | 3/4 | 1/8 | 1.41(3) |
| $a = 7.0690(2)$ Å | V, 4b | 0 | 1/4 | 3/8 | 0.38(6) |
| $c = 6.2595(3)$ Å | O1, 16h | 0 | 0.4286(7) | 0.2035(7) | 1.69(14) |
| $R_I = 0.031$; $R_p = 0.077$ | | | | | |

The room temperature photoluminescence (PL) and photoluminescence excitation (PLE) spectra of $RVO_4:Bi^{3+}$ samples are shown in Figure 6. These spectra match well with the results reported earlier for $YVO_4:Bi^{3+}$ (see e.g., [20]) and reveal a broad emission band in visible range with the maximum near 570 nm. The excitation spectrum represents a complex broad band, in which the maxima near 275 and 330 nm can be distinguished, with the excitation edge located at 350–380 nm. The emission band with maximum at 570 nm, which is independent of excitation wavelength, is believed to be caused by excitons localized near isolated Bi^{3+} ions (see [21] and references herein). Similar emission of self-trapped excitons was also observed in other complex oxide compounds (see e.g., [22,23]). The excitation band at 275 nm most probably is caused by the spin-forbidden transition of VO_4^{3-} groups ($^1A_1 \rightarrow ^1T_1$) [21,24,25], while the 330 nm band can be attributed to the metal-to-metal charge transfer transition in $Bi^{3+}-V^{5+}$ complex [21,26]. The transitions from the 1S_0 ground state to the 3P_1 excited state of Bi^{3+} ions should also contribute to the excitation band below 330 nm [27].

Besides the broad emission band at 570 nm related to Bi^{3+} , the photoluminescence spectra of the studied (Gd,Y,Lu)VO₄:Bi³⁺ samples contains also some minor lines attributed to traces of Sm^{3+} ions in the studied samples (see e.g., [28,29] for comparison). The Sm^{3+} traces most evidently came as a contamination of the equipment after earlier syntheses of some Sm-based materials. At the same time, for the LaVO₄:Bi³⁺ sample, the Bi-related emission was revealed to be of low intensity, so the

unwanted emission of Sm^{3+} impurity dominates (see Figure 6). Nevertheless, the PLE spectrum for $\text{LaVO}_4:\text{Bi}^{3+}$ is similar to these observed in other $(\text{Gd},\text{Y},\text{Lu})\text{VO}_4:\text{Bi}^{3+}$ samples.

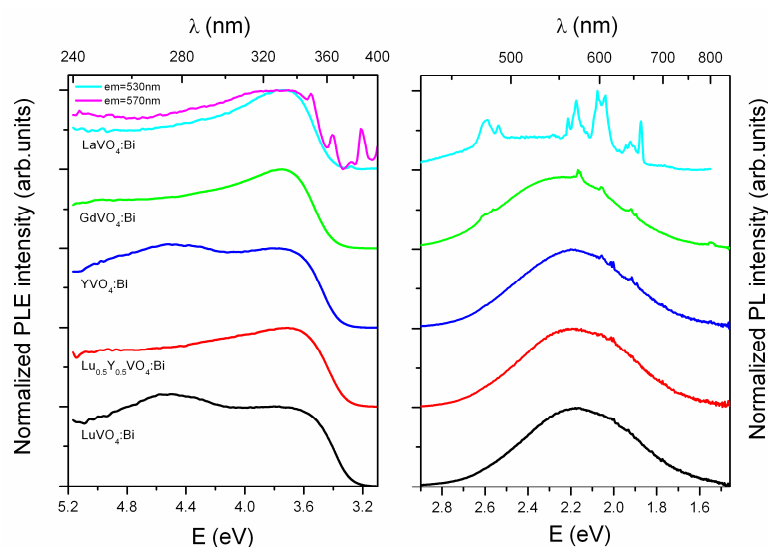


Figure 6. Normalized PLE (left) and PL (right) spectra of $R\text{VO}_4:\text{Bi}$ (1%) samples ($R = \text{La}, \text{Gd}, \text{Y}, \text{Y}_{0.5}\text{Lu}_{0.5}$ and Lu) measured at room temperature.

The washing in NaOH changes the color of the as-synthesized samples from yellowish-brown to snow-white as a result of bleaching of the broad absorption at 370–550 nm (see Figure 7 for details). Our photoluminescence quantum yield (QY) measurements testify that the Bi-doped samples washed in NaOH have got also a higher QY in comparison with the corresponding as-synthesized (yellowish) samples. For example, the QY of the $\text{YVO}_4:\text{Bi}$ at 330 nm excitation was revealed to be $36 \pm 1\%$ and $70 \pm 3\%$ for the as-synthesized and washed samples, respectively.

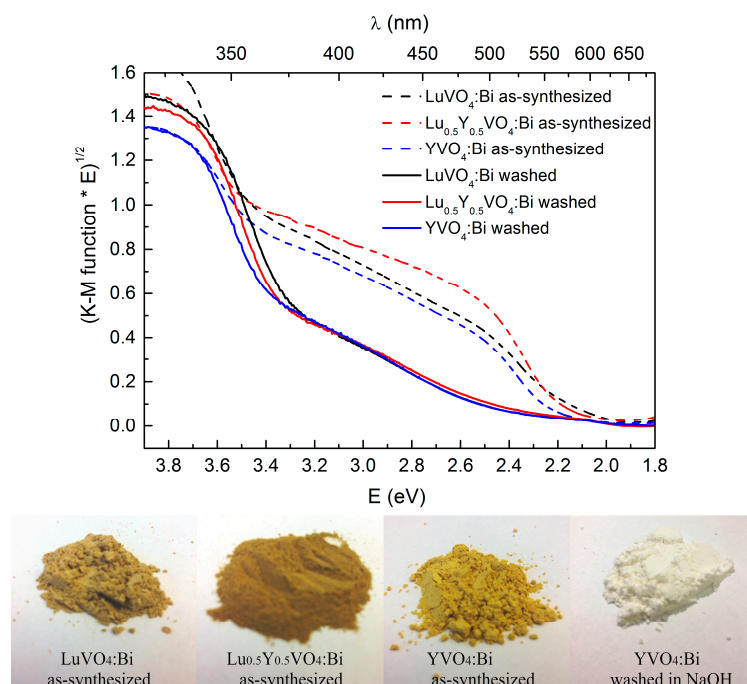


Figure 7. Comparison of the optical absorption spectra and color of $\text{YVO}_4:\text{Bi}$, $\text{Y}_{0.5}\text{Lu}_{0.5}\text{VO}_4:\text{Bi}$ and $\text{LuVO}_4:\text{Bi}$ samples, as-synthesized and washed in NaOH .

One can notice that the excitation edge position of the Bi-doped samples shifts towards higher energies with increasing of ionic radius of the rare-earth ion (from Lu^{3+} to Gd^{3+}). The precise estimation of the excitation edge position was done, as shown in Figure 8. In the case of $\text{LaVO}_4\text{:Bi}$, the excitation edge position is distorted by $f-f$ transitions of Sm^{3+} impurity observed in this particular sample (see PLE spectrum for $\text{LaVO}_4\text{:Bi}$ in Figure 6).

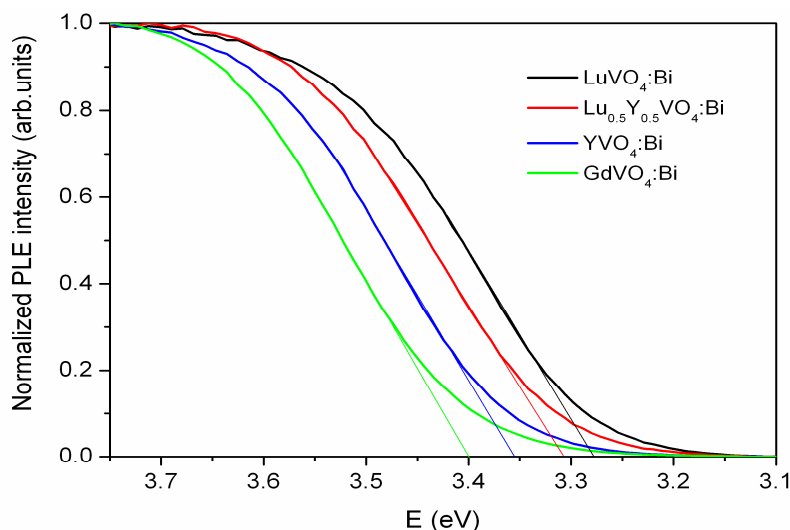


Figure 8. Estimation of the excitation edge of the Bi-related emission ($\lambda_{\text{em}} = 570 \text{ nm}$) registered in the studied $\text{RVO}_4\text{:Bi}(1\%)$ samples at room temperature.

The electronic structure calculations suggested that the valence band of the vanadates is formed mainly by $2p$ oxygen states and the bottom of the conduction band is formed by $3d$ states of vanadium [30,31]. At the same time, the $6s$ states of the bismuth ions are located slightly above the valence band of YVO_4 , while the $6p$ states of bismuth ions are included inside conduction band and are mixed with vanadium $3d$ states [26,32,33]. Therefore, the luminescence excitation edge of $\text{RVO}_4\text{:Bi}^{3+}$ can be formed by the charge transfer transitions from $6s^2$ states of Bi^{3+} to $3d^0$ states of V^{5+} ions.

The excitation edge position for the studied $\text{RVO}_4\text{:Bi}$ samples as a function of the RE ionic radius is presented in Figure 9 together with the literature data for the isostructural $(\text{Sc},\text{Y})\text{VO}_4\text{:Bi}$ materials. The excitation edge positions for Bi-doped scandium-yttrium orthovanadates were estimated similarly as in Figure 7 from the excitation spectra of $(\text{Y}_{1-y}\text{Sc}_y)\text{VO}_4\text{:Bi}$ compounds presented in Reference [6]. These results testify that the excitation edge position of the Bi-related emission, which should correlate with the energy band gap of the material, depends linearly on the RE ionic radius as well as from the V–O distance in the zircon-type RVO_4 structures. Knowing that the energy band gap in the vanadates is determined by O and V, and the V–O distances in the zircon-type vanadates are increasing with the RE ionic radius (see Figure 10), it can be assumed that the energy band gap in RVO_4 series increases gradually with the RE ionic radius increase.

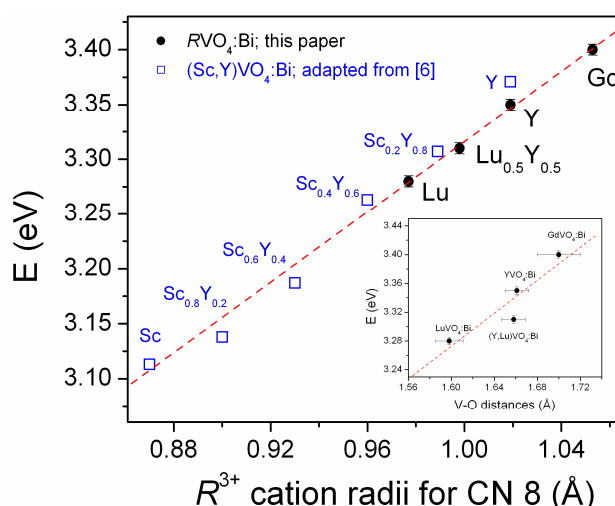


Figure 9. The room-temperature excitation edge position for the tetragonal zircon-type $RVO_4:Bi$ vanadates vs. the RE ionic radius. The solid line represents a linear fit of our data for the Bi-doped Lu, $Lu_{0.5}Y_{0.5}$, Y and Gd materials. The inset represents the excitation edge position as a function of the V–O distances in the $RVO_4:Bi$ samples studied. $LaVO_4:Bi$ drops out from this consideration because it belongs to the monoclinic monazite-type structure.

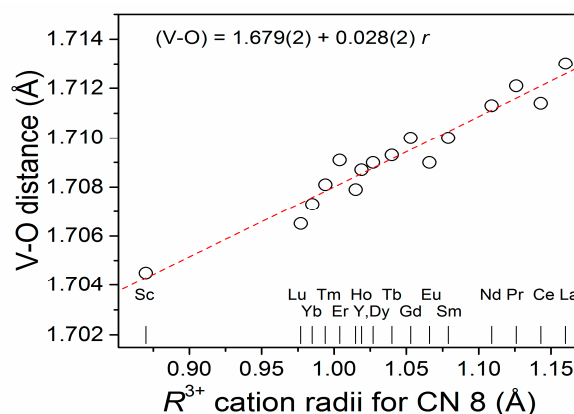


Figure 10. The V–O distances in the tetragonal zircon-type orthovanadate series as a function of eight-coordinated R^{3+} cations after Shannon [15]. Corresponding values were evaluated from the structural data of RVO_4 compounds published in References [13,34,35].

3. Materials and Methods

The studied materials were obtained in the form of nano- and submicro-crystalline powders by a standard solid-state reaction technique. For the preparation of mixed YVO_4 -based orthovanadates with nominal compositions $Y_{0.5}R_{0.5}VO_4$ ($R = Sm, Tb, Dy, Ho, Tm, Yb, Lu$), stoichiometric amounts of yttrium oxide Y_2O_3 (99.9%, Alfa Aesar, Ward Hill, MA, USA), ammonium metavanadate NH_4VO_3 (99%, LLC Sfera Sim, Lviv, Ukraine) and RE oxides (R_2O_3 and Tb_4O_7 , all 99.9%, Alfa Aesar) were carefully mixed in agate mortar, placed on alumina crucibles and heat treated in air subsequently at 1123 K for 4 h, at 1173 K for 3 h and at 1273 K for 6 h with intermediate regrinding of the product.

Similar experimental technique has been applied for a synthesis of the selected Bi^{3+} -doped vanadates. Bismuth oxide Bi_2O_3 was used as a doping precursor for preparation of the samples with nominal compositions $La_{0.99}Bi_{0.01}VO_4$, $Gd_{0.99}Bi_{0.01}VO_4$, $Y_{0.99}Bi_{0.01}VO_4$, $Lu_{0.99}Bi_{0.01}VO_4$ and $Y_{0.49}Lu_{0.50}Bi_{0.01}VO_4$ assuming that Bi substitutes RE ions. The temperature regime for synthesis of the $LaVO_4:Bi$ and $GdVO_4:Bi$ materials was the same as described above, whereas the Y- and Lu-based vanadates were prepared by heat treatment of corresponding precursors in air at 1073 K for 14 h with one intermediate regrinding of the products.

Phase composition, crystal structure and microstructural parameters of the samples were studied by means of the X-ray powder diffraction (XRD) technique. The experimental diffraction data were collected at the modernized DRON-3M diffractometer (Bourestnik, Saint Petersburg, Russia) (Cu K α -radiation) in the 2θ range 15–120° with the 2θ step of 0.02° and typical exposition 5–8 s per step. The refinement of crystal structure parameters, as well as evaluation of microstructural parameters of the powders from angular dependence of the Bragg's maxima broadening, has been performed by full profile Rietveld method using the WinCSD program package [36]. The LaB₆ external standard was used for the correction of instrumental broadening. The observed peak shapes were modelled using the pseudo-Voigt function which is a convolution of Gaussian profile and Lorentzian profile functions.

The photoluminescence (PL) and photoluminescence excitation (PLE) spectra were measured at room temperature using a Horiba/Jobin-Yvon Fluorolog-3 spectrofluorometer (Edison, NJ, USA) with a 450 W continuous xenon lamp as an excitation source and a Hamamatsu R928P PMT detector (Hamamatsu Photonics K.K., Hamamatsu City, Shizuoka, Japan) in photon counting mode. The measured PLE spectra were corrected for the xenon lamp emission spectrum. The PL spectra were corrected for the spectral response of the spectrometer system used. The photoluminescence quantum yield (QY) was evaluated as the ratio of the number of emitted photons to that of the absorbed photons similarly as it was described elsewhere [37]. The optical absorption spectra were derived from the diffuse reflectance spectra using the Kubelka-Munk transformation. The diffuse reflectance spectra of the powder samples were measured using a Varian Cary 5000 spectrophotometer (Palo Alto, CA, USA.) with external diffuse reflectance accessory DRA-2500.

4. Conclusions

The phase-pure nano- and submicro-crystalline powders of new mixed orthovanadates Y_{0.5}R_{0.5}VO₄ ($R = \text{Sm, Tb, Dy, Ho, Tm, Yb, Lu}$) and some Bi³⁺-doped RVO₄ ($R = \text{La, Gd, Y, Lu}$) materials have been prepared by a facile solid state reaction route at 1073–1273 K from the rare earth oxides and ammonium metavanadate as initial reagents and Bi₂O₃ oxide as a doping precursor. The precise crystal structure parameters including unit cell dimensions, positional and displacement parameters of atoms, as well as microstructural parameters of the powders such as average grain size and microstrains, were derived from the experimental X-ray powder diffraction data by using full-profile Rietveld refinement technique. Based on comparison of the crystal structure parameters of the new mixed orthovanadates Y_{0.5}R_{0.5}VO₄ with the parent YVO₄ and RVO₄ compounds, a formation of continuous solid solutions Y_{1-x}R_xVO₄ in the YVO₄–RVO₄ pseudo-binary systems ($R = \text{Sm, Tb, Dy, Ho, Tm, Yb, Lu}$) has been proved.

It was shown that the excitation edge position of the Bi-related emission in RVO₄:Bi orthovanadates, which correlates with the energy band gap of the materials, increases linearly with increment of the V–O distance as a result of the increasing RE ionic radius in the series from Sc³⁺ to Gd³⁺.

Author Contributions: A.T., V.H. and I.L. synthesized the samples by solid state reactions technique, contributed to the data evaluation and to the manuscript writing. L.V. performed the laboratory X-ray powder diffraction measurements, made the structural characterization of the samples and wrote the manuscript. V.T. and Y.Z. carried out the luminescence studies of the Bi-doped materials and contributed to the manuscript writing. All authors read and approved the final manuscript.

Funding: This research was funded by the Ministry of Education and Science of Ukraine (project DB/Feryt, N 0118U000264), and partially by the Polish National Science Center (project 2015/17/B/ST5/01658).

Conflicts of Interest: The authors declare no conflict of interest.

References

1. Kolitsch, U.; Holtstam, D. Crystal chemistry of REEXO₄ compounds ($X = \text{P, As, V}$). II. Review of REEXO₄ compounds and their stability fields. *Eur. J. Mineral.* **2004**, *16*, 117–126. [[CrossRef](#)]
2. Koechner, W. *Solid-State Laser Engineering*; Springer: Berlin/Heidelberg, Germany, 2006; p. 69. ISBN 978-0-387-29094-2.

3. Kalai Selvan, R.; Gedanken, A.; Anilkumar, P.; Manikandan, G.; Karunakaran, C. Synthesis and characterization of rare earth orthovanadate (RVO₄; R = La, Ce, Nd, Sm, Eu & Gd) Nanorods/Nanocrystals/Nanospindles by a facile sonochemical method and their catalytic properties. *J. Clust. Sci.* **2009**, *20*, 291–305. [[CrossRef](#)]
4. Kaminskii, A.A. Tetragonal vanadates REVO₄ (RE = Ln (Ce–Lu), Y)—A novel class of SRS-active crystals. *Dokl. Phys.* **2013**, *58*, 165–168. [[CrossRef](#)]
5. Chen, L.; Chen, K.J.; Lin, C.C.; Chu, C.I.; Hu, S.F.; Lee, M.H.; Liu, R.S. Combinatorial approach to the development of a single mass YVO₄:Bi³⁺, Eu³⁺ Phosphor with red and green dual colors for high color rendering white light-emitting diodes. *J. Comb. Chem.* **2010**, *12*, 587–594. [[CrossRef](#)] [[PubMed](#)]
6. Kang, F.; Zhang, H.; Wondraczek, L.; Yang, X.; Zhang, Y.; Lei, D.Y.; Peng, M. Band-gap modulation in single Bi³⁺-doped yttrium–scandium–niobium vanadates for color tuning over the whole visible spectrum. *Chem. Mater.* **2016**, *28*, 2692–2703. [[CrossRef](#)]
7. Liu, H.; Yuan, J.; Jiang, Z.; Shangguan, W.; Einaga, H.; Teroaka, Y. Novel photocatalyst of V-based solid solutions for overall water splitting. *J. Mater. Chem.* **2011**, *21*, 16535–16543. [[CrossRef](#)]
8. Huang, X.Y.; Wang, J.X.; Yu, D.C.; Ye, S.; Zhang, Q.Y. Spectral conversion for solar cell efficiency enhancement using YVO₄:Bi³⁺, Ln³⁺ (Ln = Dy, Er, Ho, Eu, Sm, and Yb) phosphors. *J. Appl. Phys.* **2011**, *109*, 113526. [[CrossRef](#)]
9. Errandonea, D.; Garg, A.B. Recent progress on the characterization of the high-pressure behaviour of AVO₄ orthovanadates. *Prog. Mater. Sci.* **2018**, *97*, 123–169. [[CrossRef](#)]
10. International Centre for Diffraction Data (ICDD). *PDF-4+ 2010 (Database)*; Kabekkodu, S., Ed.; International Centre for Diffraction Data: Newtown Square, PA, USA, 2010.
11. Isasi, J.; Veiga, M.L.; Laureiro, Y.; Saez-Puche, R.; Pico, C. Synthesis, structural determination and magnetic behavior of Y_xGd_{1-x}VO₄ phases (x = 0.25, 0.50, 0.75). *J. Alloys Compd.* **1991**, *177*, 143–147. [[CrossRef](#)]
12. Milligan, W.O.; Vernon, L.W. Crystal Structure of Heavy metal orthovanadates. *J. Phys. Chem.* **1952**, *56*, 145–148. [[CrossRef](#)]
13. Chakoumakos, B.C.; Abraham, M.M.; Boatner, L.A. Crystal structure refinements of zircon-type MVO₄ (M = Sc, Y, Ce, Pr, Nd, Tb, Ho, Er, Tm, Yb, Lu). *J. Solid State Chem.* **1994**, *109*, 197–202. [[CrossRef](#)]
14. Aldred, A.T. Cell Volumes of APO₄, AVO₄ and ANbO₄ Compounds, where A = Sc, Y, La–Lu*. *Acta Crystallogr. B* **1984**, *40*, 569–574. [[CrossRef](#)]
15. Shannon, R.D. Revised effective ionic radii and systematic studies of interatomic distances in halides and chalcogenides. *Acta Crystallogr. A* **1976**, *32*, 751–757. [[CrossRef](#)]
16. Rice, C.E.; Robinson, W.R. Lanthanum orthovanadate. *Acta Crystallogr. B* **1976**, *32*, 2232–2233. [[CrossRef](#)]
17. Takeshita, S.; Ogata, H.; Isobe, T.; Sawayama, T.; Niikura, S. Effects of citrate additive on transparency and photostability properties of YVO₄:Bi³⁺, Eu³⁺ nanoposphor. *J. Electrochem. Soc.* **2010**, *157*, J74. [[CrossRef](#)]
18. Garces, N.Y.; Stevens, K.T.; Foundos, G.K.; Halliburton, L.E. Electron paramagnetic resonance and optical absorption study of V⁴⁺ centres in YVO₄ crystals. *J. Phys. Condens. Matter* **2004**, *16*, 7095–7106. [[CrossRef](#)]
19. Cooper, J.K.; Scott, S.B.; Ling, Y.; Yang, J.; Hao, S.; Li, Y.; Toma, F.M.; Stutzman, M.; Lakshmi, K.V.; Sharp, I.D. Role of Hydrogen in Defining the *n*-Type Character of BiVO₄ Photoanodes. *Chem. Mater.* **2016**, *28*, 5761–5771. [[CrossRef](#)]
20. Datta, R. Bismuth in yttrium vanadate and yttrium europium vanadate phosphors. *J. Electrochem. Soc.* **1967**, *114*, 1057–1063. [[CrossRef](#)]
21. Cavalli, E.; Angiuli, F.; Mezzadri, F.; Trevisani, M.; Bettinelli, M.; Boutinaud, P.; Brik, M.G. Tunable luminescence of Bi³⁺-doped YP_xV_{1-x}O₄ (0 ≤ x ≤ 1). *J. Phys. Condens. Matter* **2014**, *26*, 385503. [[CrossRef](#)] [[PubMed](#)]
22. Zazubovich, S.; Krasnikov, A.; Zorenko, Y.; Gorbenko, V.; Babin, V.; Mihokova, E.; Nikl, M. Luminescence of Pb- and Bi-Related Centers in Aluminum Garnet, Perovskite, and Orthosilicate Single-Crystalline Films. In *Nanocomposite, Ceram. Thin Film Scintill*; Nikl, M., Ed.; Pan Stanford Publishing: Singapore, 2017; pp. 227–302. ISBN 978-981-4745-22-2.
23. Krasnikov, A.; Luchechko, A.; Mihokova, E.; Nikl, M.; Syvorotka, I.I.; Zazubovich, S.; Zhydachevskii, Y. Origin of Bi³⁺-related luminescence in Gd₃Ga₅O₁₂:Bi epitaxial films. *J. Lumin.* **2017**, *190*, 81–88. [[CrossRef](#)]
24. Barendswaard, W.; Weber, R.T.; van der Waals, J.H. An EPR study of the luminescent triplet state of VO³⁻₄ in YVO₄ and YP_{0.96}V_{0.04}O₄ single crystals at 1.2 K. *J. Chem. Phys.* **1987**, *87*, 3731. [[CrossRef](#)]
25. Matos, M.; Rocha, L.; Nassar, E.; Verelst, M. Influence of Bi³⁺ ions on the excitation wavelength of the YVO₄:Eu³⁺ matrix. *Opt. Mater.* **2016**, *62*, 12–18. [[CrossRef](#)]

26. Boutinaud, P. Revisiting the spectroscopy of the Bi^{3+} ion in oxide compounds. *Inorg. Chem.* **2013**, *52*, 6028–6038. [[CrossRef](#)] [[PubMed](#)]
27. Blasse, G.; Brill, A. Investigations on Bi^{3+} -Activated Phosphors. *J. Chem. Phys.* **1968**, *48*, 217–222. [[CrossRef](#)]
28. Atuchin, V.V.; Aleksandrovsky, A.S.; Chimitova, O.D.; Diao, C.P.; Gavrilova, T.A.; Kesler, V.G.; Molokeyev, M.S.; Krylov, A.S.; Bazarov, B.G.; Bazarova, J.G.; et al. Electronic structure of $\beta\text{-RbSm}(\text{MoO}_4)_2$ and chemical bonding in molybdates. *Dalton Trans.* **2015**, *44*, 1805. [[CrossRef](#)] [[PubMed](#)]
29. Atuchin, V.V.; Aleksandrovsky, A.S.; Molokeyev, M.S.; Krylov, A.S.; Oreshonkov, A.S.; Zhou, D. Structural and spectroscopic properties of self-activated monoclinic molybdate $\text{BaSm}_2(\text{MoO}_4)_4$. *J. Alloys Compd.* **2017**, *729*, 843–849. [[CrossRef](#)]
30. Panchal, V.; Errandonea, D.; Segura, A.; Rodriguez-Hernandez, P.; Muoz, A.; Lopez-Moreno, S.; Bettinelli, M. The electronic structure of zircon-type orthovanadates: Effects of high-pressure and cation substitution. *J. Appl. Phys.* **2011**, *110*, 043723. [[CrossRef](#)]
31. Garg, A.B.; Errandonea, D.; Rodrigues-Hernandez, P.; Munoz, A. ScVO_4 under non-hydrostatic compression: A new metastable polymorph. *J. Phys. Condens. Matter* **2017**, *29*, 055401. [[CrossRef](#)] [[PubMed](#)]
32. Dolgos, M.R.; Paraskos, A.M.; Stoltzfus, M.W.; Yarnell, S.C.; Woodward, P.M. The electronic structures of vanadate salts: Cation substitution as a tool for band gap manipulation. *J. Solid State Chem.* **2009**, *182*, 1964–1971. [[CrossRef](#)]
33. Mahlik, S.; Amer, M.; Boutinaud, P. Energy level structure of Bi^{3+} in Zircon and Scheelite polymorphs of YVO_4 . *J. Phys. Chem. C* **2016**, *120*, 8261–8265. [[CrossRef](#)]
34. Mullica, D.F.; Sappenfield, E.L.; Abraham, M.M.; Chakoumakos, B.C.; Boatner, L.A. Structural investigations of several LnVO_4 compounds. *Inorg. Chim. Acta* **1996**, *248*, 85–88. [[CrossRef](#)]
35. Oka, Y.; Yao, T.; Yamamoto, N.J. Hydrothermal synthesis of lanthanum vanadates: Synthesis and crystal structures of zircon-type LaVO_4 and a new compound LaV_3O_9 . *Solid State Chem.* **2000**, *152*, 486–491. [[CrossRef](#)]
36. Akselrud, L.; Grin, Yu. WinCSD: Software package for crystallographic calculations (Version 4). *J. Appl. Crystallogr.* **2014**, *47*, 803–805. [[CrossRef](#)]
37. Zhydachevskyy, Y.; Syvorotka, I.I.; Tsiumra, V.; Baran, M.; Lipińska, L.; Wierzbicka, A.; Suchocki, A. Quantum efficiency of the down-conversion process in $\text{Bi}^{3+}\text{-Yb}^{3+}$ and $\text{Ce}^{3+}\text{-Yb}^{3+}$ co-doped garnets. *Sol. Energy Mater. Sol. Cells* **2018**, *185*, 240–251. [[CrossRef](#)]



© 2018 by the authors. Licensee MDPI, Basel, Switzerland. This article is an open access article distributed under the terms and conditions of the Creative Commons Attribution (CC BY) license (<http://creativecommons.org/licenses/by/4.0/>).